

Accepted Manuscript

Title: Tungstophosphoric acid supported on mesoporous niobiumoxophosphate: An efficient solid acid catalyst for etherification of 5-hydroxymethylfurfural to 5-ethoxymethylfurfural

Authors: P. Krishna Kumari, B. Srinivasa Rao, D. Dhana Lakshmi, N. Ruthwik Sai Paramesh, C. Sumana, N. Lingaiah

PII: S0920-5861(18)30858-7
DOI: <https://doi.org/10.1016/j.cattod.2018.06.047>
Reference: CATTOD 11536

To appear in: *Catalysis Today*

Received date: 20-3-2018
Revised date: 15-6-2018
Accepted date: 30-6-2018

Please cite this article as: Kumari PK, Rao BS, Dhana Lakshmi D, Sai Paramesh NR, Sumana C, Lingaiah N, **Tungstophosphoric acid supported on mesoporous niobiumoxophosphate: An efficient solid acid catalyst for etherification of 5-hydroxymethylfurfural to 5-ethoxymethylfurfural**, *Catalysis Today* (2018), <https://doi.org/10.1016/j.cattod.2018.06.047>

This is a PDF file of an unedited manuscript that has been accepted for publication. As a service to our customers we are providing this early version of the manuscript. The manuscript will undergo copyediting, typesetting, and review of the resulting proof before it is published in its final form. Please note that during the production process errors may be discovered which could affect the content, and all legal disclaimers that apply to the journal pertain.



Tungstophosphoric acid supported on mesoporous niobiumoxophosphate: An efficient solid acid catalyst for etherification of 5-hydroxymethylfurfural to 5-ethoxymethylfurfural

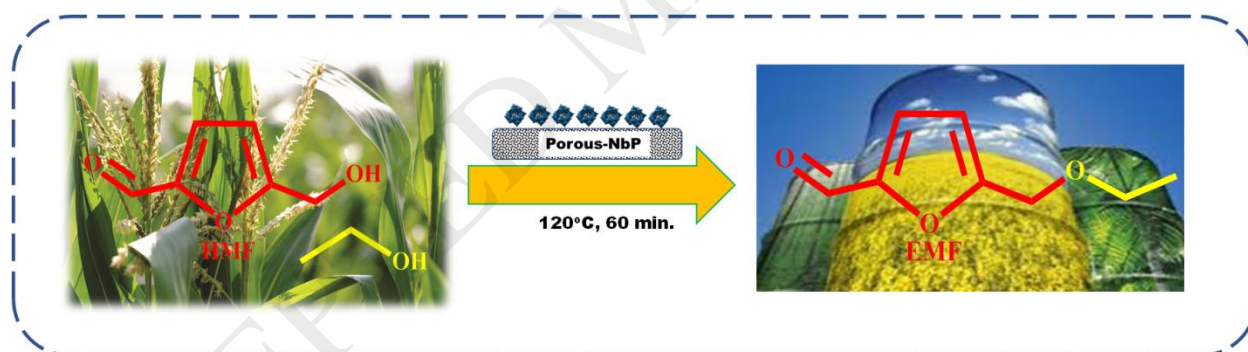
P. Krishna Kumari,¹ B. Srinivasa Rao,¹ D. Dhana Lakshmi,¹ N. Ruthwik Sai Paramesh,²
C. Sumana,² N. Lingaiah^{1*}

¹Department of Catalysis & Fine Chemicals and ²Chemical Engineering
CSIR-Indian Institute of Chemical Technology, Hyderabad-500 007, Telangana, India.

*Corresponding author. Tel.: +91 40 27191722; fax: +91 40 27160921

E-mail address: nakkalingaiah@iict.res.in (N. Lingaiah).

Graphical abstract



The research highlights:

- TPA supported on niobium phosphate is active catalyst for selective conversion of HMF to EMF
- The NbOPO₄ and TPA contribute to both Lewis and Bronsted acidic sites
- Activity of the catalysts depends on the amount and dispersion of TPA on support
- The activity of the catalysts depends on nature of support and heteropoly acid.

Abstract

Tungstophosphoric (TPA) supported on mesoporous niobiumoxophosphate (NbP) catalysts were prepared with different loadings. The synthesized materials employed as heterogeneous solid acid catalysts for selective etherification of 5-hydroxymethylfurfural to 5-ethoxymethylfurfural. Physico-chemical properties of the catalysts were obtained by different spectroscopic techniques and their results exposed that TPA was a highly dispersed state on NbP and acidity of the catalyst enhanced due to its dispersion. The higher catalytic performance can be allied to the total acidity of the catalysts with appropriate number of Brønsted-Lewis acid sites which were directed by the contact and dispersion of TPA on support. Different reaction parameters were premeditated and 25 wt% TPA/NbP catalyst exhibited highest catalytic activity with 95% of HMF conversion and 89% of EMF yield. The catalyst is reusable without noticeable turn down in catalytic performance up to five cycles. A kinetic model for etherification of HMF was also derived.

Keywords: 5-Hydroxymethylfurfural; 5-Ethoxymethylfurfural; Etherification; Niobiumoxo phosphate, Heteropolyacids; Tungstophosphoric acid.

1. Introduction

Biorefinery will play a key role for current urge of fuels, energy and chemical backbone materials which used for a broad range of applications without compromising the desires of upcoming generations [1]. Depletion of fossil fuel reserves and their negative impact on the

planet has put pressure on the society to build up a new; ecofriendly and long term sustainable chemical sources [2, 3]. Biomass is one of hopeful renewable choice for this intention. Biomass is made up of hemicelluloses, cellulose and lignin [4]. Cellulose and hemicelluloses can be converted into carbohydrates [5]. These carbohydrates can be valorized into platform molecules such as 5-hydroxymethylfurfural (HMF), furfuryl alcohol and levulinic acid [6, 7]. Among many chemicals HMF with two functional groups, combined with the furan ring, makes as an appealing elementary unit for different value-added products. Furan derivatives has wide range of applications in different sectors has been used as biofuels (dimethylfuran, 5-ethoxymethylfurfural) [8, 9], monomer units (2, 5-diformylfuran and 2, 5-furandicarboxylic acid) [10, 11] and other fine chemicals.

Among all HMF derivatives 5-ethoxymethylfurfural (EMF) has eminent fuel properties, used as an excellent biofuel additive [12]. EMF has high energy density (8.7 kWh/L), which is nearly close to the regular diesel and it also has high cetane number, which is important property for combustion of fuel. Moreover, in engine tests EMF blend with regular diesel generates less SO₂ emissions and soot [13]. Beverage industries used EMF as a flavoring representative due to its low toxicity [14]. The byproduct ethyl levulinate (EL) formed throughout the production of EMF also has a significant biodiesel property which is also used as blending constituent in biodiesel [15, 16].

To date, different routes were proposed by using various substrates sources such as hexoses, 5-hydroxymethylfurfural and 5-(chloromethyl) furfural (CMF) for the preparation of EMF. The conversion of fructose to EMF was achieved using Ar-SO₃H-SBA-15 catalyst and obtained about 63.4% of EMF yield at 116 °C after 4 h [17]. Mesoporous carbon with SO₃H functional groups used for direct synthesis of EMF from fructose at 140 °C after 24 h with

55.7% yield [18]. Hu Li *et al.* achieved relatively more efficient yield of EMF around 76.6% from fructose after 15 h of reaction time at 120 °C in mixed solvent (EtOH/DMSO) with the use of acid–base hybrid nanospheres of TPA and amino acid catalyst [19]. Different catalysts such as SO₃H-functionalized mesoporous carbon [20], MCM-41-HPW [21], MIL-101-SO₃H [22] also studied for the synthesis of EMF from fructose. In sequence to produce EMF in desirable yield from fructose, longer reaction time and higher temperatures are essential. Moreover, mixture of solvent system obligatory to gets an attractive yield of EMF. Even though, halo methyl furfural (For example CMS) reported higher yields of EMF, but concern to hazardous nature of HCl produced by nucleophilic replacement of Cl with ethanol and this route is not virtuous [23]. Definitely synthesis of EMF from hexoses was interesting pathway as it is cost effective and one pot strategy. Still there are some drawback which has to overcome long reaction time, high catalyst loadings and low yields of EMF. In this scenario the selective synthesis of EMF from 5-HMF considered as more interesting path way as it offers less reaction times, catalyst loadings and high selectivity. Direct synthesis of EMF from HMF is more preferable as the quantitative yield can be achieved. Inorganic salts, mineral acids [24], Fe₃O₄@SiO₂-HPW [25], heteropolyacids (HPAs) dispersed on different supports like K-10 clay [26], H₄SiW₁₂O₄₀/MCM-41 nanospheres [27], ZrO₂/SBA-15 [28], cellulose derived carbon treated with sulfuric acid catalysts [29] were showed high amount of EMF yield at longer reaction times. Sulfated silica and sulfuric acid functionalized polymer materials were also used for HMF conversion to EMF but the activity was limited [30, 31]. Lanzafame *et al.* [32] conducted HMF etherification over MCM-41 catalysts, including Al-MCM-41 (with different Si/Al ratio), zirconia over SBA-15, and sulfated zirconia-SBA- 15. On the other hand, Barbera *et al.* [33] introduced NH₄-exchanged zeolites for HMF etherification with moderate EMF yield of 60%.

Development of efficient catalytic system for the selective synthesis of EMF is highly desirable. Along with different promising acid catalysts, heteropolyacids (HPAs) have strong Brønsted acidity and proton mobility can be good candidates for acid catalyzed reactions like etherification, benzylation and esterification reactions [34]. However, solubility nature of HPAs in polar solvents creates problem in separation of catalyst from reaction mixture. To overcome these drawbacks HPAs are made into heterogeneous by exchanging the protons with metal ions like Cs^+ , Ag^+ , and Ti^{+4} [35, 36] or dispersing them on different supports with acidic character like zeolite, niobia, metal phosphates etc. [37-42]. In comparison to metal oxides, metal phosphates are more acidic and can be expected to give better catalytic performance when these are used as supports for HPAs.

Mesoporous niobiumoxophosphate (NbP) was used as support for dispersion of HPAs. A series of TPA dispersed on NbP catalysts were synthesized and their catalytic performance evaluated towards the selective conversion of HMF to EMF. The catalysts were characterized by different methods to derive their surface properties and corroborated with their catalytic activity.

2. Experimental

2.1. Catalyst preparation

The chemicals used in the preparation of catalysts purchased from Aldrich. TPA dispersed on mesoporous NbP catalysts were prepared as following [43]. First mesoporous NbP was prepared by using hexadecylamine (90%) as a template. In a usual synthesis, about 2.30 g of

H₃PO₄ (85% aqueous solution) was added to the partially hydrolyzed 2.73 g of NbCl₅ (99%) in 50 mL of water followed by extra 50 mL of water was added and stirred for another 30 min. The mixture was adjusted to pH of 2.6 by adding ammonia solution. After stirring, the slurry was filtered and washed the gel with deionized water to get a chlorine-free gel. About 1.45 g of hexadecylamine dissolved in 50 mL of water and stirred until clear solution was obtained. Then the filtered gel was added to this solution and stirred for 60 min. Finally, 0.92 g H₃PO₄ (85%) was added to the mixture solution and adjusted the pH of the mixture to 3.9. Then the slurry was kept for hydrothermal treatment in a teflon-lined stainless-steel autoclave at 110 °C for 48 h. The as-synthesized NbP was filtered, washed with deionized water and dried at 100 °C for 12 h. The template free mesoporous NbP was obtained by calcining at 500 °C for 6 h under air flow. The obtained solid NbP used as support.

Finally, a series of catalysts with different TPA loadings (5-30 wt %) dispersed on NbP were prepared by wet impregnation method. A wanted amount of TPA dissolved in water was added to the mesoporous NbP and the resulting mixture was kept on hot plate at 70 °C until to remove excess water. Then, the dried samples were further dried overnight at 100 °C and calcined at 300 °C for 2 h to obtain final catalysts.

2.2. Characterization methods

Powder X-ray diffraction patterns of the synthesized catalysts were acquired on an Ultima-IV diffractometer of Rigaku Corporation, Japan equipped with Ni-filtered Cu K α radiation ($\lambda=1.54056 \text{ \AA}$) handled at 30 kV and 15 mA with a scan speed of 2° min^{-1} and a scan range of 10–80°.

The acidic strength of the solid catalysts was measured by temperature programmed desorption of ammonia (NH₃-TPD) was carried on BELCAT-II (Belsorb, Japan). About 50 mg of the catalyst was pre-treated at 300 °C for 1 h in a flow of pure helium (99.9%, 30 mL min⁻¹). Eventually, the catalyst was soaked with 10% NH₃/He at 100 °C for 1 h then flushed with He at the same temperature for the complete removal of physisorbed ammonia. Then the TPD profile was continued while increasing the temperature from 100 °C to 800 °C with a ramp rate of 10 °C min⁻¹. The desorbed NH₃ was monitored with thermal conductivity detector (TCD).

Fourier transform IR spectra of the catalysts were recorded on a DIGILAB (USA) IR spectrometer using the KBr disc method.

Pyridine adsorbed FT-IR spectroscopy used for the examination of characteristic nature of the acid sites in DRIFT mode at room temperature. In the typical experiment the catalyst was degassed under vacuum at 200 °C for 3 h followed by suspending dry pyridine. Then, the excess pyridine was removed by heating the sample at 120 °C for 1 h. After cooling the sample to room temperature, FT-IR spectra of the pyridine-adsorbed samples were recorded.

The BET surface area, pore volume and pore sizes were determined by N₂ adsorption-desorption method using BELSorb II Instrument, Japan at liquid nitrogen temperature. Before measurement the samples were degassed at 200 °C for 2 h.

2.3. Etherification of HMF

The catalytic etherification of HMF with ethanol was performed in a sealed tubular reactor. In a typical experiment HMF (0.126 g) was dissolved in ethanol (2 g) and catalyst (3.8 wt% with respect to reaction mixture) were charged into the sealed tubular reactor and immersed in an oil bath under controlled temperature range (80-140 °C). After a particular period of time,

the reactor was removed and cooled the reaction mixture to room temperature. Subsequently, the catalyst was separated from reaction mixture by centrifugation and the collected sample mixture was diluted with ethanol. Reaction samples were analyzed by gas chromatograph (Shimadzu 2010) equipped with a flame ionization detector (FID). The products were separated by an innowax capillary column (diameter: 0.25 mm, length: 30 m) and confirmed the products by GC-MS (Shimadzu, GCMSQP2010S) analysis.

3. Results and discussion

3.1. Characterization

XRD patterns of the pure NbP and TPA loaded NbP catalysts are displayed in the Fig. 1. The support NbP exhibited two broad peaks at 2θ of 25.53° and 51.8° [44, 45]. Low intense diffraction patterns related to Keggin ion of TPA were appeared for the catalysts with above 20 wt% of TPA on NbP [46]. The intensity of patterns related to TPA increased with increase in the content of TPA. The XRD results indicate that TPA was highly dispersed at lower loadings.

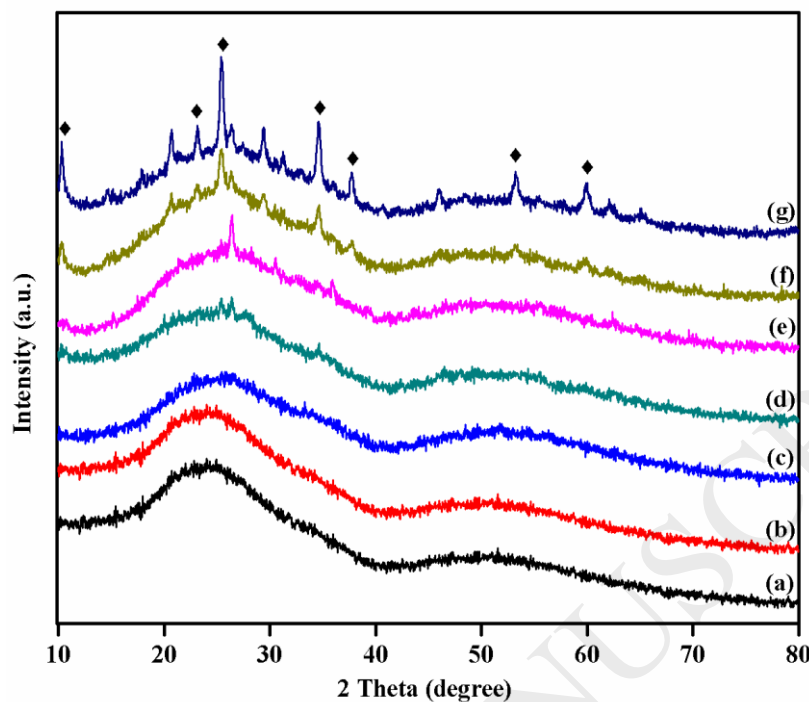


Fig. 1. XRD patterns of TPA/NbP catalysts. (a) NbP (b) 5 (c) 10 (d) 15 (e) 20 (f) 25 (g) 30 wt% TPA/NbP (◆) TPA.

FT-IR spectra of TPA/NbP samples are depicted in Fig. 2. The Nb–O–P band in NbP catalyst have vibrational band at 1180 cm^{-1} [47] and TPA characteristic IR bands generally appear at 1082 , 980 , 870 cm^{-1} [48]. It was clearly visible that TPA supported on NbP samples had vibrational band at 1180 cm^{-1} , signifying the existence of Nb–O–P system in all the prepared catalysts. The intensity of band at 1180 cm^{-1} increased with raising the content of TPA on NbP. It may be due to the merging of P–O band in TPA with Nb–O–P band in NbP. All the TPA containing catalysts have characteristic bands at 870 cm^{-1} (W–O–W) and the band at 980 cm^{-1} ($\text{W}=\text{O}_{\text{terminal}}$) was increased with increase in TPA loading indicating the presence of TPA on NbP.

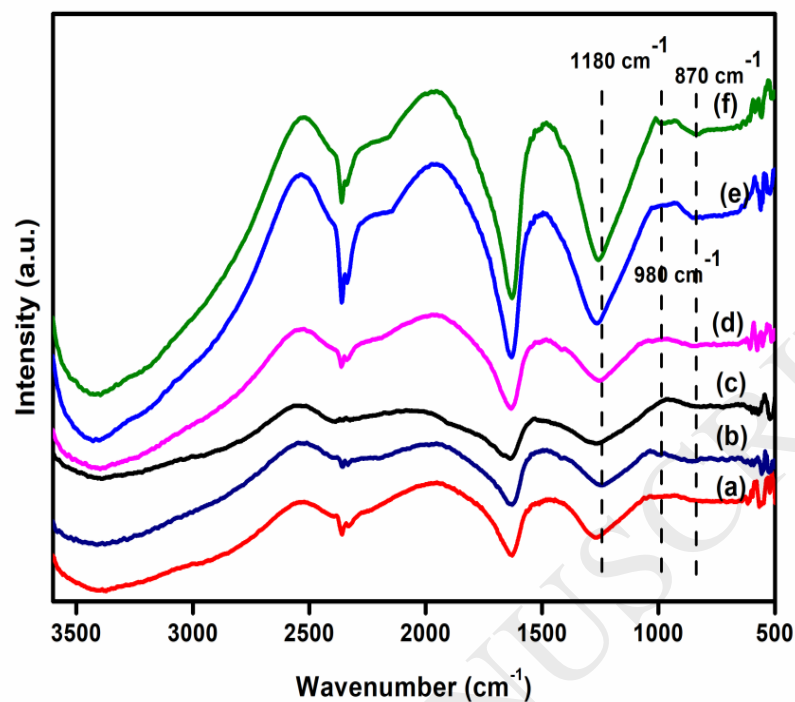


Fig. 2. FT-IR spectra of TPA/NbP catalysts. (a) 5 (b) 10 (c) 15 (d) 20 (e) 25 (f) 30 wt% TPA/NbP

Py-FTIR spectra employed for the examination of types of acidic sites present in the catalysts are shown in Fig. 3. The samples showed bands at 1450 cm⁻¹, 1540 cm⁻¹, 1490 cm⁻¹, which were attributed to Lewis acid sites, Brønsted acid sites and combination of both Brønsted and Lewis acid sites respectively. The NbP support showed more Lewis acid sites, which could be generated by the presence of NbO₆ (octahedral) and NbO₄ (tetrahedral) and low Brønsted acid sites could be generated by Nb-OH and P-OH species present on the mesoporous NbP support [47]. When NbP loaded with TPA more Brønsted acid sites were generated by the protons present in TPA [49] and the concentration of these sites was improved gradually with increasing the content of TPA from 5-30 wt%. These results indicate that the catalysts contain both Lewis and Brønsted acid sites.

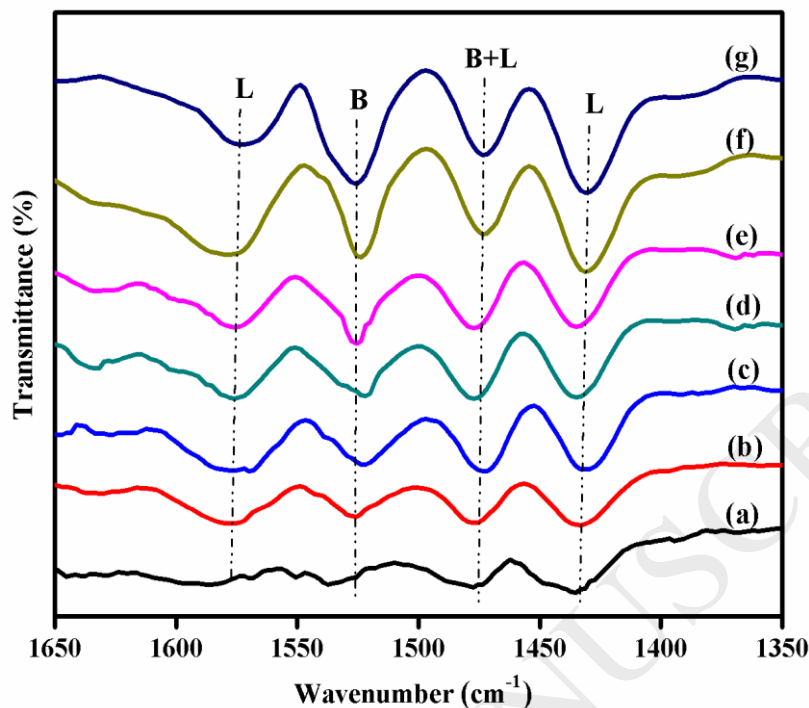


Fig. 3. Py-IR spectra of TPA/NbP catalysts. (a) NbP (b) 5 (c) 10 (d) 15 (e) 20 (f) 25 (g) 30 wt% TPA/NbP.

NH₃-TPD technique employs for the determination of strength of the acidic sites present on the catalyst surface and total quantity of acidic sites. Ammonia adsorption-desorption profiles of the catalysts are publicized in Fig. 4 and their corresponding acidic strength values are provided in Table 1. The acidity values of the catalysts increased with increasing in TPA loading and reached to a maximum for 25 wt% of TPA loading. Further increase in TPA content beyond 25 wt% there was no noticeable increase in acidity. All the prepared catalysts showed a broad desorption peak in the region of 140–450 °C, which are unresolved. As the TPA content increased in the catalyst, a high temperature desorption peak appeared at around 550 °C. The low temperature desorption peak mainly originating from support NbP which are mostly Lewis acidic sites. The intensities of these Lewis acidic peaks decreased with TPA loading. The high

temperature desorption peak was due to the ammonia adsorbed on strong Bronsted acidic sites of the catalyst.

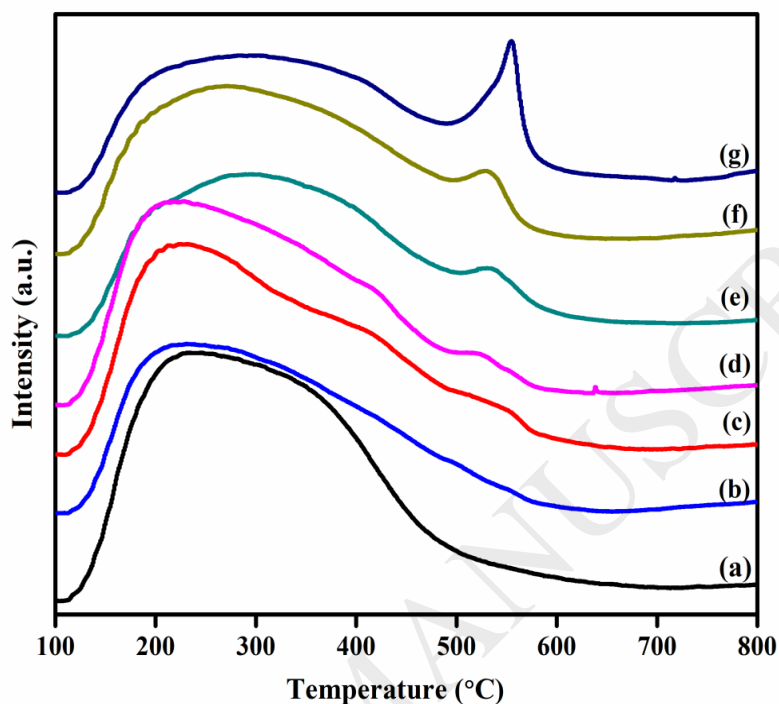


Fig. 4. NH₃-TPD profiles of TPA/NbP catalysts. (a) NbP (b) 5 (c) 10 (d) 15 (e) 20 (f) 25 (g) 30 wt% TPA/NbP.

Textural properties of NbP, bulk TPA and TPA dispersed on NbP catalysts are listed in Table 1. Compared with parent NbP support, surface area (S_{BET}) of TPA/NbP catalysts was decreased with variation of TPA loading. These features resulted due to the deposition of TPA species inside the pores of the support and are finely dispersed on the surface of support, leading to the partial blockage of the adsorption sites on the surface of NbP. However, it was clearly indicated that surface area (S_{BET}) of support and prepared TPA/NbP catalysts demonstrate a high surface area than bulk TPA ($S_{\text{BET}} = 8.5\text{m}^2\text{ g}^{-1}$). The surface density (SD) was calculated for the TPA/NbP catalysts and shown in the Table 1.

Table 1. Acidity values and Textural properties of the TPA/NbP samples.

Catalyst	Weak-Moderate acidity (m.mol/g)	Strong acidity (m.mol/g)	Total acidity (m.mol/g) ^a	S _{BET} (m ² g ⁻¹) ^b	SD ^c (KU/nm ²)
NbP	1.230	-	1.230	233	
5 wt% TPA/NbP	1.257	0.086	1.343	185	0.05
10 wt% TPA/NbP	1.366	0.102	1.468	160	0.13
15 wt% TPA/NbP	1.326	0.154	1.480	141	0.22
20 wt% TPA/NbP	1.480	0.185	1.665	125	0.33
25 wt% TPA/NbP	1.435	0.260	1.695	114	0.45
30 wt% TPA/NbP	1.125	0.351	1.476	60	1.04

^aTotal acidity of catalysts measured by NH₃-TPD, ^bBET Surface area. ^cSD-surface density of Keggin unit (KU)

Surface densities are accounted as the number of Keggin units per surface area (KU/nm²). The SD is increased with TPA loading. The theoretical monolayer coverage of Keggin clusters is 0.7 KU/nm² [50] and that the Keggin clusters may behave similar to bulk TPA crystallites as surface densities increase beyond monolayer coverage (>0.7 KU/nm²). The Combined results from XRD analysis and surface density values, it could be indicative that TPA was highly dispersed over the surface of NbP at lower loadings of TPA [51, 52].

3.2. Activity of TPA/NbP catalysts

The catalytic etherification of HMF results are shown in Table 2. When the reaction was done without catalyst HMF did not convert to EMF. The support NbP as catalyst HMF conversion was only 9.4% with 9% of EMF yield. For assessment of catalytic activity of parent TPA reaction was done with pure TPA. TPA presented almost total HMF conversion with 83% of EMF and 17% of EL yield. Though, TPA represented better activity towards HMF conversion it is soluble in the reaction mixture. The reaction was accomplished with a series of TPA/NbP catalysts. The catalyst with 5 wt% TPA on NbP able to convert 43.8% of HMF with 42% of EMF yield. When increase in TPA loading up to 25 wt% over NbP, a significant increase in the conversion and yield was observed. The maximum EMF yield of 89% with 95.2% HMF conversion was observed for 25 wt% TPA/NbP catalyst within 60 min. When TPA content is beyond 25 wt% HMF conversion was increased and at the same time a decrease in EMF yield was noticed. The divergence in activity of catalyst was owed to the decrease in total acidity with more number of strong acidic sites other than reasonable number of weak-moderate and strong acidic sites for the catalysts with above 25 wt% TPA loading on NbP. Presence of more number of strong acidic sites in 30 wt% TPA/NbP catalyst encouraged further conversion of EMF to EL. The high yield with high conversion was noticed for the 25 wt% TPA/NbP catalyst. This catalyst has highest total acidity with reasonable number of weak-moderate and strong acidic sites and these are favoring high activity of the catalyst. The activity results are in fit with the acidity profiles of NH_3 -TPD. The results established that the catalytic presentation of these TPA/NbP catalysts is not only directly associated to the total acidity but also nature of acidic sites and TPA dispersion on NbP support.

Table 2: Etherification of HMF to EMF over TPA/NbP catalysts.

Catalyst	HMF	Yield (%)	
	Conversion (%)	EMF	EL
Without catalyst	-	-	-
NbP	9.4	9	0.4
5 wt% TPA/NbP	43.8	42	1.8
10 wt% TPA/NbP	67.0	64	3.0
15 wt% TPA/NbP	74.6	71	3.6
20 wt% TPA/NbP	83.0	78	5.0
25 wt% TPA/NbP	95.2	89	6.2
30 wt% TPA/NbP	97.0	89	8.0
TPA	100.0	83	17.0

Reaction conditions: HMF: 0.126 g; Catalyst wt%: 3.76; Ethanol: 2 g; Temperature: 120 °C; Time: 60 min.

The catalytic performance of TPA/NbP catalyst was compared with different acid catalysts towards the etherification of HMF to EMF. Bing Liu et al. reported alumina grafted K-10 clay [26] catalyst for the preparation of EMF and it showed high efficiency towards the EMF (89.5%) from HMF at 100 °C after 8 h of reaction time. Fe₃O₄@SiO₂-HPW [25] and 40 wt% MCM-41-HPW [27] catalysts were given 84 and 83% of EMF respectively. Yongshen Ren et al.

proposed partially exchanged silver phosphotungstic acid ($\text{Ag}_1\text{H}_2\text{PW}$) [35] as a right catalyst for EMF synthesis and they obtained 88.7% of EMF yields at 100 °C of reaction temperature after 10 h. Sulfated carbon material [29] as a catalyst and produced 84.4% of EMF yields at 100 °C after 6 h. Even though these catalytic systems gave efficient yields of EMF still they need longer reaction times (6 to 10 h) than the present TPA/NbP catalyst which showed high activity within one hour. TPA/NbP catalyst gave 89% of EMF yields within 60 min of reaction time. The efficient catalytic activity of TPA/NbP catalysts was due to the existence of appropriate number of surface acid sites with both Lewis-Brønsted acidity and well dispersion of TPA on the NbP.

3.3. Effect of catalyst weight

Under identical conditions catalyst weight played a significant effect on the conversion of HMF to EMF. The effect of catalyst weight was studied, and results are recorded in Fig. 5. The availability of the number of active sites was increased with increasing the catalyst weight, in order that the conversion of HMF and EMF yields were also increased with increasing the catalyst weight. When the catalyst weight was 0.94 wt%, the HMF conversion was 56.4% with EMF yield of 54%. Further increase in catalyst weight from 0.94 to 3.76 wt%, HMF conversion reached about 95.2% with 89% of EMF yield. When the dosage of catalyst further increased to 4.70 wt%, HMF conversion was increased, while the EMF yield was decreased marginally. The decrease in the EMF yield was due to the excess amount of catalyst encouraged the further conversion of EMF to EL along with conversion of HMF to EMF. So, 3.76 wt% of catalyst was the right quantity to get more EMF yield.

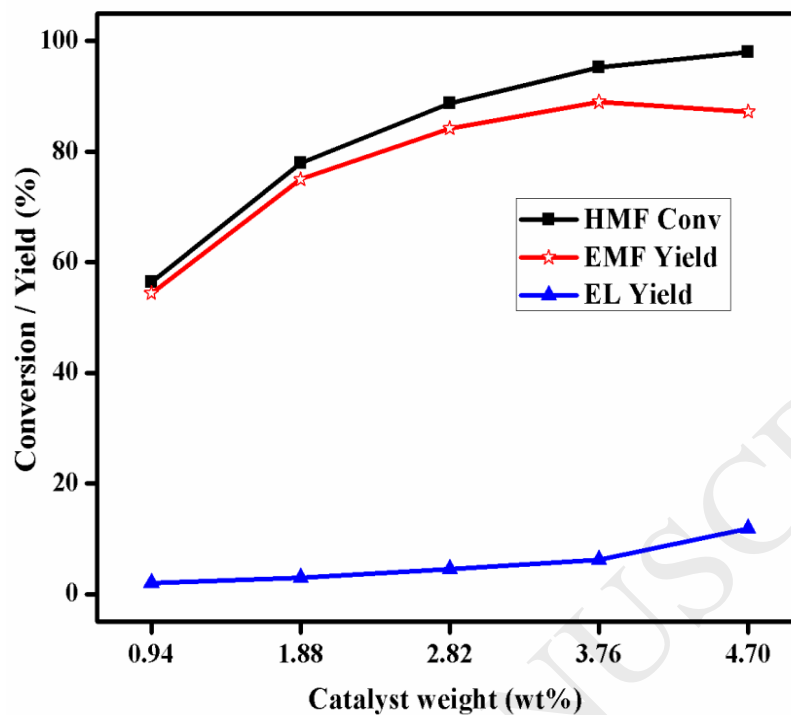


Fig. 5: Results of selective etherification of HMF to EMF with variation in catalyst loading. Reaction conditions: HMF: 0.126 g; Catalyst: 25 wt% TPA/NbP; Ethanol: 2 g; Temperature: 120 °C; Time: 60 min.

3.4. Effect of reaction temperature

Influence of the reaction temperature towards the conversion of HMF to EMF over TPA/NbP catalyst was studied in the temperature range 80 to 140 °C and illustrated the results in Fig. 6. When the reaction was performed at 80 °C the conversion of HMF was 50% with 48.6% of EMF yield. Consequently; with further increase in the reaction temperature to 100 and 120 °C the HMF conversion and EMF yields were also increased drastically. It was found that HMF conversion reached to 95.2% with 89% of EMF yield at 120 °C. When performed the reaction at 140 °C, the conversion of HMF was increased to 99% with a decrease in EMF yield from 89% to 84.6%. The optimum reaction temperature was fixed at 120 °C for further experiments.

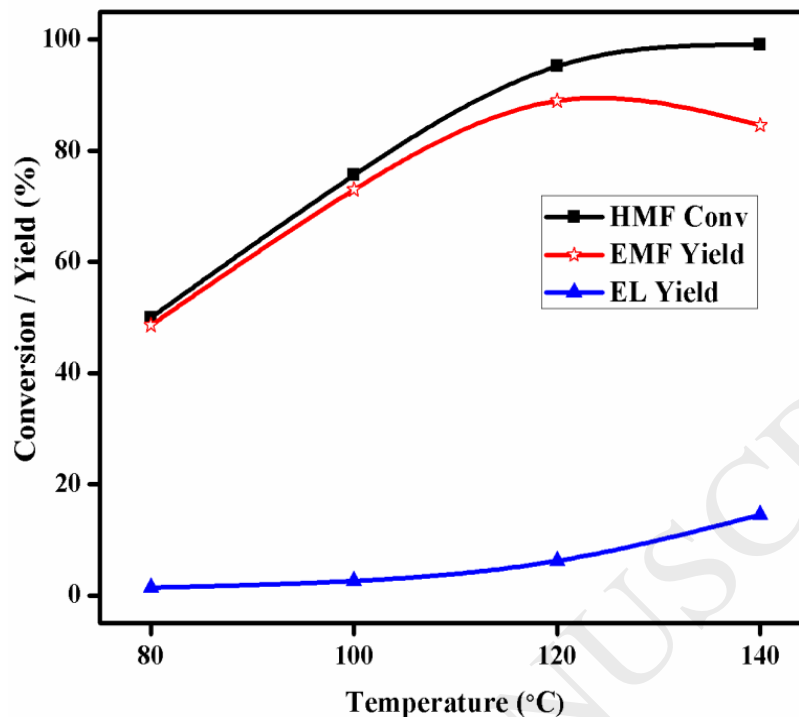


Fig. 6: Influence of reaction temperature on HMF etherification over 25 wt% TPA/NbP catalyst. Reaction conditions: HMF: 0.126 g; Catalyst wt%: 3.76; Ethanol: 2 g; Time: 60 min.

3.5. Effect of reaction time

Effect of the reaction time on the etherification of HMF was studied and the results are summarized in Fig. 7. The conversion of HMF and EMF yields were increased with increase in reaction time from 15 to 60 min. At early 15 min of reaction time the HMF conversion was 58% with 54% of EMF yield. When the reaction time prolonged to 60 min HMF conversion increased to 95.2% with 89% of EMF yield. Further experiment progressed up to 90 min, HMF conversion was increased to 98% with a decrease in EMF yield from 89 to 86%. It revealed that etherification of HMF to EMF and further alcoholysis of EMF to EL was taking place simultaneously and the products were also confirmed by NMR spectroscopy. The optimum reaction time for obtaining high yield is 60 min.

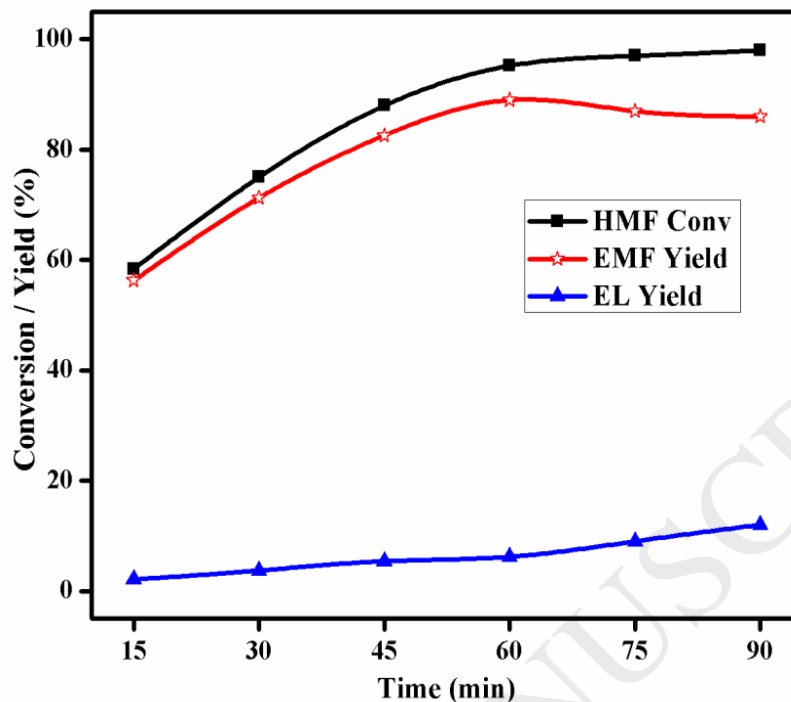
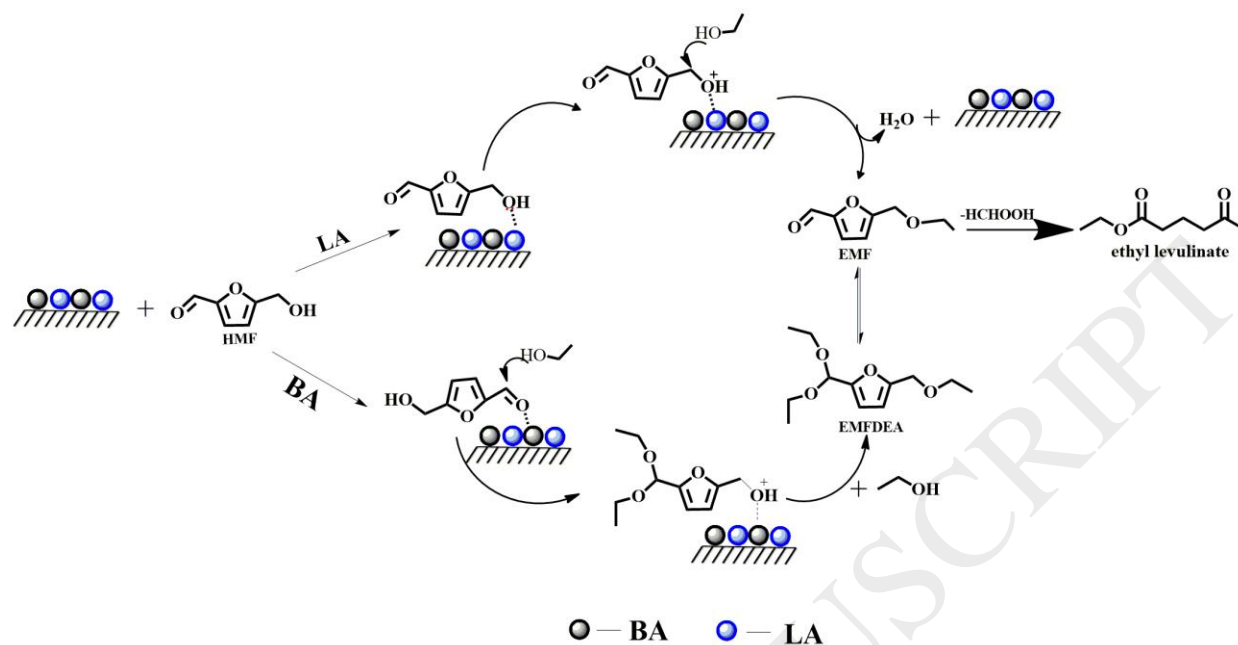


Fig. 7: Effect of reaction time on HMF etherification over 25 wt% TPA/NbP catalyst.

Reaction conditions: HMF: 0.126 g; Catalyst wt%: 3.76; Ethanol: 2 g; Temperature: 120 °C

Based on aforementioned results from time effect a plausible reaction mechanism was proposed as shown in Scheme 1. As the present catalyst has both Bronsted and Lewis acidic sites the reaction goes through two possible ways. In the presence of Bronsted acidity (BA), EMF formation obtained via acetal intermediate. The formation was observed with the analysis of GCMS [53]. The Lewis acidic sites (LA) might interact with the hydroxyl group of HMF molecule to form EMF (direct etherification) [54]. With the prolonged reaction time furan ring of EMF opening followed by the exclusion of formic acid led to form ethyl levulinate.



Scheme 1: Plausible reaction mechanism for catalytic etherification of HMF to EMF

3.6. Effect of substrate concentration on reaction

The effect of HMF concentrations on the conversion of HMF to EMF were examined over 25 wt% TPA/NbP at constant ethanol (2g) amount. The effect of HMF concentration on the conversion of HMF to EMF is shown in Fig. 8. When the reaction was performed with 0.063 g of HMF the yield of EMF was 87.6% with 98% of HMF conversion. When the amount of HMF increased to 0.126 g the yield of EMF was increased up to 89% with 95.2% HMF conversion. Further increase in the concentration of HMF from 0.126 g to 0.378 g the yield of EMF and HMF conversion was decreased. At lower concentration of HMF, these molecules react with sufficiently available catalytic active sites to form EMF along with few amount of side products 5-(diethoxymethyl)-2-furanmethanol (EMFDEA) and ethyl levulinate (EL). The side product

EMFDEA was minimum at low HMF concentration and dimerization of HMF was observed at high HMF concentrations (above 0.126 g).

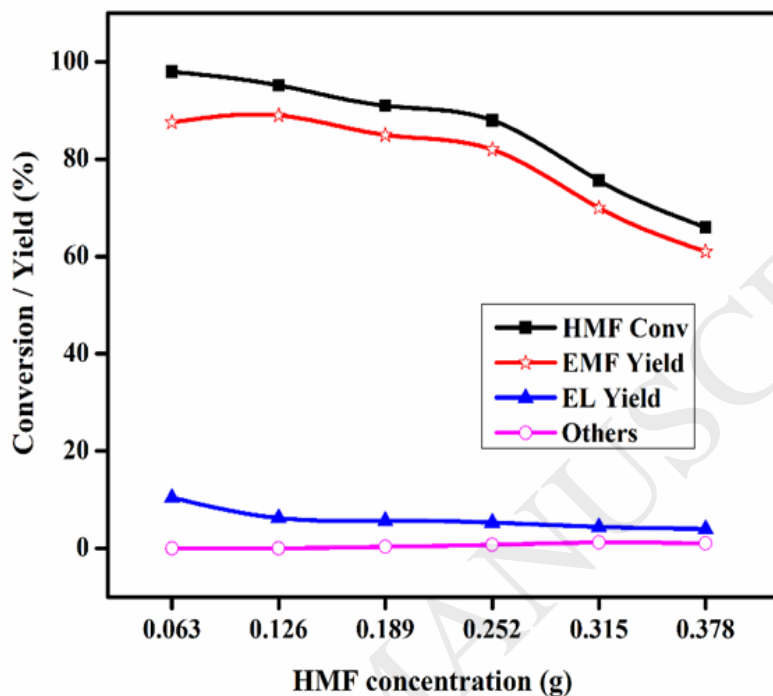


Fig. 8: Effect of HMF concentration on the etherification of HMF to EMF over 25 wt%

TPA/NbP catalyst

Reaction conditions: HMF: 0.126 g; Catalyst wt%: 3.76; Ethanol: 2 g, Temperature: 120 °C; Time: 60 min.

3.7. Activity of different HPAs supported on NbP

After screening of a sequence of TPA/NbP catalysts for etherification of HMF to EMF, the catalytic performance of other heteropolyacids (HPAs) supported on NbP also evaluated. The activity results of TPA, silicotungsticacid (STA) and molybdophosphoricacid (MPA) supported on NbP catalysts and total acidity values are presented in Table 3. The activity of HPAs towards the etherification of HMF to EMF follows the order TPA>STA>MPA. Among the

heteropolyacids, TPA showed superior activity and MPA exhibited least activity. STA gave better activity than MPA. The variations in the activity of HPAs were due to difference in their acidity values as shown in Table 3. The acidity of HPAs decreased as follows TPA>STA>MPA. The evaluated study indicates that acidity of HPAs played a key role for selective etherification of HMF to EMF.

Table 3. Catalytic activity results of different HPAs supported on NbP support.

Catalyst	HMF Conversion (%)	Yield (%)		Acidity (mmol/gm)
		EMF	EL	
25 wt% TPA/NbP	95.2	89.0	6.2	1.695
25 wt% STA/NbP	81.6	77.6	4.0	0.930
25 wt% MPA/NbP	65.2	62.0	3.2	0.530

Reaction conditions: HMF: 0.126 g; Catalyst wt%: 3.76; Ethanol: 2 g; Temperature: 120 °C; Time: 60 min.

3.8. Activity of TPA supported on different supports.

The activity of TPA supported on different metal oxide supports such as ZrO₂, Nb₂O₅ and SiO₂ for etherification of HMF is shown in Table 4. The acidity and surface area of these supports was different and showed dissimilarity in their activity. The performance of TPA dispersed on different supports follows the order of TPA/NbP>TPA/SiO₂>TPA/Nb₂O₅>TPA/ZrO₂. Here TPA/NbP performed highest activity due to the well dispersion of TPA on the prepared NbP support along with acidity. NbP as a support has more surface area with acidity

than other supports. The experimental activity results noticed that both surface area and acidity of the support responsible for highest HMF etherification activity.

Table 4. Catalytic activity results of TPA supported on different supports.

Catalyst	HMF Conversion (%)	Yield (%)		Acidity (mmol/gm)
		EMF	EL	
25 wt% TPA/ZrO ₂	34.7	33.7	1.0	0.130
25 wt% TPA/Nb ₂ O ₅	43.0	41.0	2.0	0.410
25 wt% TPA/SiO ₂	60.2	56.2	4.0	0.570
25 wt% TPA/NbP	95.2	89.0	6.2	1.695

Reaction conditions: HMF: 0.126 g; Catalyst wt%: 3.76; Ethanol: 2 g; Temperature: 120 °C; Time: 60 min.

3.9. Recycle experiments of TPA/NbP catalysts

In sequence to find reusability and stability of the present catalyst, the reaction was carried at 120 °C with 3.76 wt% of catalyst for 60 min of reaction time. After completion of the experiment, the spent catalyst was recovered from reaction mixture by centrifugation and washed with ethanol. The recovered catalyst was dried at 110 °C and used for the next cycle of the reaction under equivalent experimental conditions. The process was repeated for five times and the results are depicted in Fig. 9. It was observed that the yields of EMF were constant around 87%. These results proved that the TPA/NbP catalyst is stable and reusable without

significant loss of catalytic activity. The recycled catalyst was characterized with XRD and the results were compared with the fresh catalyst (Fig. 10). No structural changes were observed for the reused catalyst.

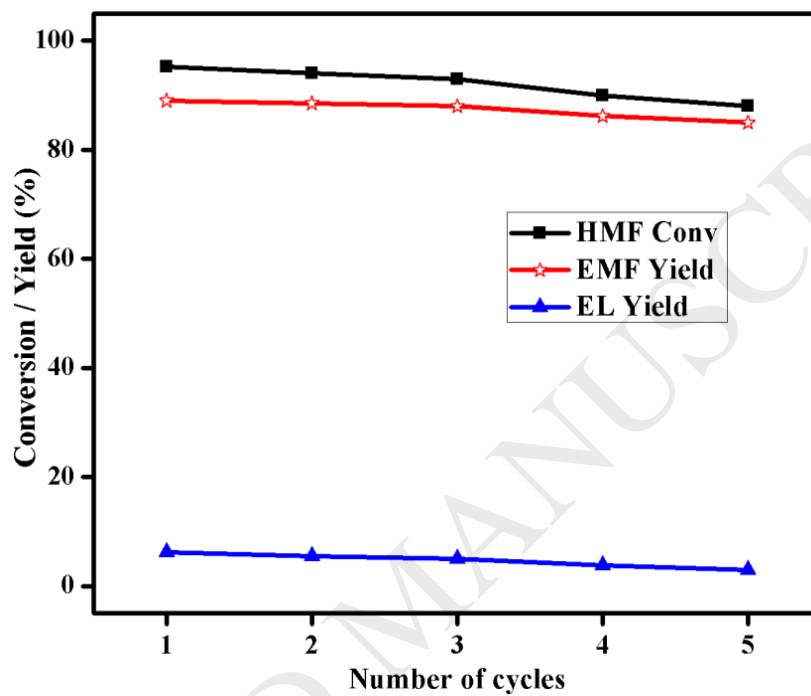


Fig. 9: Results of recycle experiments over TPA/NbP catalyst.

Reaction conditions: HMF: 0.126 g; Catalyst wt%: 3.76; Ethanol: 2 g; Temperature: 120 °C;
Time: 60 min.

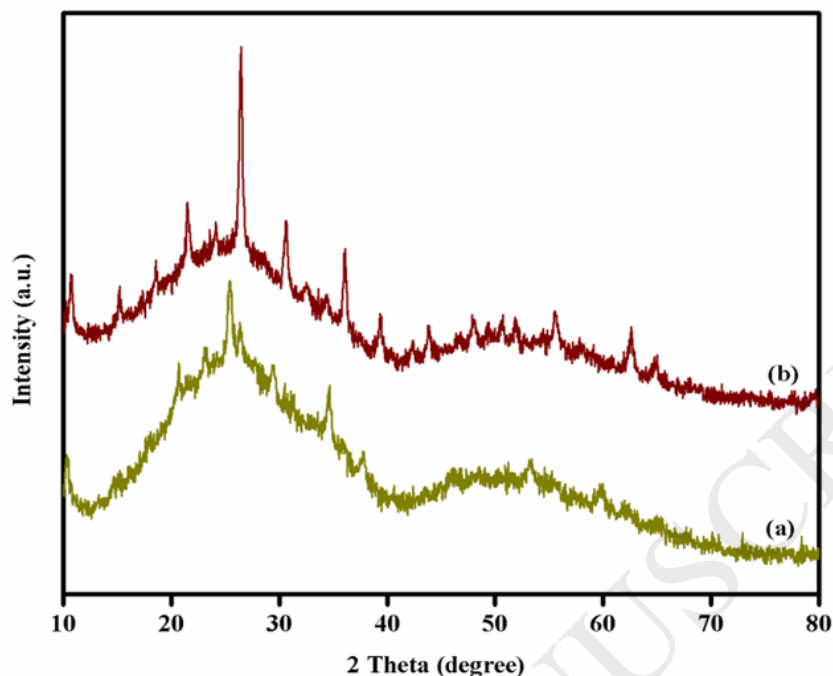
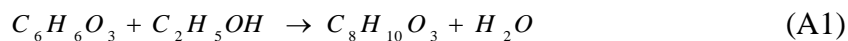


Fig. 10: XRD patterns of 25 wt% TPA/NbP catalysts (a) used (b) fresh

4. Kinetics Study

The etherification of HMF with ethanol as a reactant cum solvent proceeds via dehydration to give EMF followed by the removal of formic acid from EMF to give byproduct ethyl levulinate. The stoichiometric reactions are given by the Eqs (A1, A2) and it was observed in the present study that there was a very negligible formation of by-products. In the kinetic study of HMF etherification with EtOH using Amberlyst-15 catalyst, the mechanism of acetalization of HMF was considered prior to direct etherification [53]. However, in case of the proposed TPA/NbP catalysts, direct etherification was preferred over acetalization due to the high acidic nature of the catalyst caused by the large number of Lewis acid sites. Similar trend was observed in the case of Al-MFI zeolite catalysts [54].





The overall HMF etherification to EMF was considered and a simple power-law model/Arrhenius equation was chosen for kinetic analysis. Although the power-law model is primarily employed for homogeneous non-catalytic reactions, it can also be used for solid catalytic reactions for obtaining the preliminary value of rate parameters [55, 56]. Similar model has been considered by Sacia et al in the kinetic study of EtOH on HMF etherification using Amberlyst-15 catalyst [55]. The justification for choosing this model was as follows. It was ensured through adequate stirring in the reactor that there exist no heat and mass transfer effects that influence the kinetics of the reaction. In addition, temperature gradients in the case of liquid phase systems are not so prevalent compared to vapor phase, as heat capacities and thermal conductivities of the liquid phase are an order of magnitude higher compared to the gas phase [55]. The present etherification also being a liquid phase reaction, no significant effect of heat transfer phenomena on reaction kinetics was considered. The power-law model was deemed fit to calculate the rate parameters with the use of minimal experimental data. The rate equation for HMF etherification to EMF is given as follows:

$$-r_{HMF} = kC_{HMF}^a C_{EtOH}^b ; k = k_o e^{-E_a/RT} \quad (B2)$$

where, k is the rate constant, a & b are the respective apparent orders of the reaction w.r.t. HMF and EtOH, k_o is the pre-exponential factor, E_a is the activation energy, R is the universal gas constant and T is the reaction temperature.

It is noted that, in certain higher concentration ranges of a reactant, the reaction rate becomes independent of its concentration and hence the reactions are of zero order [57]. Similarly, in the present study, as EtOH was taken much in excess compared to the other reactant HMF, the apparent order of reaction w.r.t EtOH (b) was considered to be zero. Similar basis was

considered by Sacia et al, in the kinetic study of EtOH on HMF etherification using Amberlyst-15 catalyst [53].

Experimental study was carried out to evaluate the influence of concentration of HMF and reaction temperature on the kinetics of HMF etherification. The HMF concentration was varied from 0.063-0.378 g in intervals of 0.063 g and the pertaining yield and conversion percentages were calculated. The reaction conditions considered were 120 °C temperature, 60 min reaction time, 3.76 wt% (80 mg) catalyst and 2 g ethanol. From the given data, concentration of HMF (mol/lit) and the rate of HMF conversion ($mol/lit.m.sec.g\ cat$) were calculated. The natural logarithmic values of the concentration and rate of dissipation of HMF were plotted as shown in Fig. 11(a). From the slope of the graph, the resulted value of 'a' was $0.7977 \approx 0.8$. Further, the temperature dependency of rate constant k was studied by conducting the reaction at different temperatures within the range of 80-140 °C. The graph between $\ln k$ and $1/T$ was plotted as shown in Fig. 11(b). From the linear graph, the intercept has resulted K_o to be $0.72796\ L\ mol^{-1}\ s^{-1}$ and the slope has resulted E_a to be $14049.1547\ J/mol$.

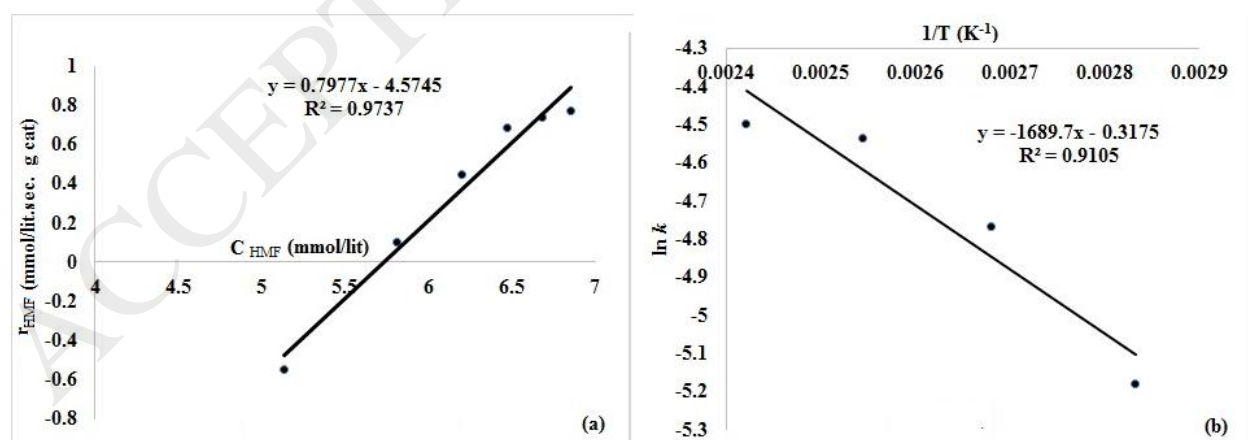


Fig. 11 (a) Apparent reaction order w.r.t. HMF; (b) Arrhenius plot for the formation of EMF

5. Conclusions

NbP supported tungstophosphoric acid catalysts were prepared with retention of Keggin ion structure. The etherification of HMF to EMF was examined over TPA/NbP catalysts, among the catalysts 25 wt% TPA/NbP catalyst showed high activity towards EMF. The activity of the catalysts depends on amount of TPA dispersed on NbP, which directs the overall acidity of the catalyst. The conversion and yields were also depending on the reaction temperature, reaction time and amount of catalyst. Further, a kinetic model for HMF etherification with the present catalyst was derived. The catalyst is easy to recover and reusable without any appreciable loss in activity.

Acknowledgements

Author P. K. Kumari acknowledge to UGC-New Delhi, India for financial support in the form of Junior Research Fellowship.

References

- [1] G. R. Gomes, D. S. Rampon, L. P. Ramos, *Appl. Catal. A: Gen.*, 545 (2017) 127–133.
- [2] Y. Zhang, J. Wang, X. Li, X. Liu, Y. Xia, B. Hu, G. Lu, Y. Wang, *Fuel*, 139 (2015) 301–307.
- [3] A. J. Ragauskas, C. K. Williams, B. H. Davison, G. Britovsek, J. Cairney, C. A. Eckert, W. J. Frederick Jr., J. P. Hallett, D. J. Leak, C. L. Liotta, J. R. Mielenz, R. Murphy, R. Templer, T. Tschaplinski, *Science*, 311 (2006) 484–489.

- [4] G. W. Huber, S. Iborra, A. Corma, *Chem. Rev.*, 106 (2006) 4044–4098.
- [5] R. M. West, E. L. Kunkes, D. A. Simonetti, J. A. Dumesic, *Catal. Today*, 147 (2009) 115–125.
- [6] M. J. Climent, A. Corma, S. Iborra, *Green Chem.*, 13 (2011) 520–540.
- [7] M. Bicker, J. Hirth, H. Vogel, *Green Chem.*, 5 (2003) 280–284.
- [8] R. Goyal, B. Sarkar, A. Bag, N. Siddiqui, D. Dumbre, N. Lucas, S. K. Bhargava, A. Bordoloi, *J. Catal.*, 340 (2016) 248–260.
- [9] Gruter GJM, Manzer LE, U.S. Patent Appl., US2010/0058650; 2010.
- [10] A. Iriondo, A. Mendiguren, M. B. Güemez, J. Reques, J. F. Cambra, *Catal. Today*, 279 (2017) 286–295.
- [11] D. X. M.-Vargas, J. R. D. L. Rosa, L. S.-Rangel, J. L. G.-Mar, Marco A. G.-Navarro, Carlos J. L.-Ortiz, David A. D. H.-D. Río, *Appl. Catal. A: Gen.*, 547 (2017) 132–145.
- [12] M. Mascal, E. B. Nikitin, *Angew. Chem.*, 120 (2008) 8042–8044.
- [13] C. M. Lew, N. Rajabbeigi, M. Tsapatsis, *Ind. Eng. Chem. Res.*, 51 (2012) 5364–5366.
- [14] H. O. E. Silva, P. G. D. Pinho, B. P. Machado, T. Hogg, J. C. Marques, J. S. Camara, F. Albuquerque, Antonio C., S. Ferreira, *J. Agric. Food Chem.*, 56 (2008) 11989–96.
- [15] K. Y. Nandiwale, S. K. Sonar, P. S. Niphadkar, P. N. Joshi, S. S. Deshpande, V. S. Patil, V. V. Bokade, *Appl. Catal. A: Gen.*, 460–461 (2013) 90–98.
- [16] L. Peng, L. Lin, J. Zhang, J. Shi, S. Liu, *Appl. Catal. A: Gen.*, 397 (2011) 259–265.
- [17] G. Morales, M. Paniagua, J.A. Melero, J. Iglesias, *Catal. Today*, 279 (2017) 305–316.
- [18] J. Wang, Z. Zhang, S. Jin, X. Shen, *Fuel*, 192 (2017) 102–107.
- [19] H. Li, K. S. Govind, R. Kotni, S. Shunmugavel, A. Riisager, S. Yang, *Energy Convers. Manage.*, 88 (2014) 1245–1251.

- [20] J. Wang, Z. Zhang, S. Jin, X. Shen, *Fuel*, 192 (2017) 102–107.
- [21] A. Liu, Z. Zhang, Z.F. Fang, B. Liu, K. Huang, *J. Ind. Eng. Chem.*, 20 (2014) 1977–1984.
- [22] X. Liu, H. Li, H. Pan, H. Zhang, S. Huang, K. Yang, W. Xue, S. Yang, *J. Energy Chem.*, 25 (2016) 523–530.
- [23] I. Viil, A. Bredihhin, U. Maeorg, L. Vares, *RSC Adv.*, 4 (2014) 5689-5693.
- [24] B. Liu, Z. Zhang, K. Huang, Z. Fang, *Fuel*, 113 (2013) 625–631.
- [25] S. G. Wang, Z. H. Zhang, B. Liu, J. L. Li, *Catal. Sci. Technol.*, 3 (2013) 2104–2112.
- [26] A. Liu, B. Liu, Y. Wang, R. Ren, Z. Zhang, *Fuel*, 117 (2014) 68–73.
- [27] P. Che, F. Lu, J. Zhang, Y. Huang, X. Nie, J. Gao, J. Xu, *Bioresour. Technol.*, 119 (2012) 433–436.
- [28] P. Lanzafame, D. M. Temi, S. Perathoner, G. Centi, A. Macario, A. Aloise, G. Giordano. *Catal. Today*, 175 (2011) 435–441.
- [29] B. Liu, Z. Zhang, K. Huang, *Cellulose*, 20 (2013) 2081–2089.
- [30] B. Liu, Z. Zhang, *RSC Adv.*, 3 (2013) 12313–12319.
- [31] H. Li, Q. Zhang, S. Yang, *Ind. J. Chem. Eng.*, 2014 (2014) 1–7.
- [32] P. Lanzafame, D. M. Temi, S. Perathoner, G. Centi, A. Macario, A. Aloise, *Catal. Today*, 175 (2011) 435-441.
- [33] S. Dutta, S. De, M. I. Alam, M. M. Abu-Omar, B. Saha. *J. Catal.*, 288 (2012) 8-15.
- [34] Ch. R. Kumar, Srinivas M., N. Lingaiah. *Appl. Catal. A: Gen.*, 487 (2014) 165–171.
- [35] Y. Ren, B. Liu, Z. Zhang, J. Lin, *J. Ind.Eng. Chem.*, 21 (2015)1127–1131.
- [36] S. Rao B., K. Kumari P., D. Lakshmi D., Lingaiah N., *Catal. Today*,
<http://dx.doi.org/10.1016/j.cattod.2017.05.040>.
- [37] I. M. Baltork, M. Moghadam, S. Tangestaninejad, V. Mirkhani, S. F. Hojati, *Polyhedron*, 27

- (2008) 750–758.
- [38] A. E. R. S. Khder, H. M. A. Hassan, M. S. E.-Shall, *Appl. Catal. A: Gen.*, 411–412 (2012) 77–86.
- [39] K. Srilatha, N. Lingaiah, B. L. A. P. Devi, R. B. N. Prasad, S. Venkateswar, P. S. S. Prasad, *Appl. Catal. A: Gen.*, 365 (2009) 28–33.
- [40] J. A. Monge, B. E. Bakkali, G. Trautwein, S. Reinoso, *Appl. Catal. B, Environ.*, 224 (2018) 194–203.
- [41] D. P. Das, K. M. Parida, *Appl. Catal. A: Gen.*, 305 (2006) 32–38.
- [42] D. P. Das, K. M. Parida, *J. Mol. Catal. A: Chem.*, 253 (2006) 70–78.
- [43] G. S. Rao, N. P. Rajan, V. Pavankumar and K. V. R. Chary, *J. Chem. Technol. Biotechnol.*, DOI 10.1002/jctb.4273.
- [44] Z. Miao, Z. Li, J. Zhao, W. Si, J. Zhou, S. Zhuo, *Mol. Catal.*, 444 (2018) 10–21.
- [45] Q. Sun, D. Fang, S. Wang, J. Shen, A. Auroux, *Appl. Catal. A: Gen.*, 327 (2007) 218–225.
- [46] G. Raveendra, M. Srinivas, N. Pasha, A. V. P. Rao, P. S. Sai Prasad, N. Lingaiah, *Reac. Kinet. Mech. Cat.*, DOI 10.1007/s11144-015-0868-6.
- [47] Y. Zhang, J. Wang, J. Ren, X. Liu, X. Li, Y. Xia, G. Lu, Y. Wang, *Catal. Sci. Technol.*, 2 (2012) 2485–2491.
- [48] B. S. Rao, P. K. Kumari, D. Dhanalakshmi, N. Lingaiah, *J. Mol. Catal. A: Chem.*, 427 (2017) 80–86.
- [49] P. K. Kumari, B. S. Rao, D. Padmakar, N. Pasha, N. Lingaiah, *Mol. Catal.*, 448 (2018) 108–115.
- [50] H. Liu, E. Iglesia, *J. Phys. Chem. B* 107 (2003) 10840–10847.
- [51] X. Kong, S. Wu, L. Liu, S. Li, J. Liu, *Mol. Catal.*, 439 (2017) 180–185.

- [52] Z. Miao, H. Zhao, H. Song, L. Chou, *RSC Adv.*, 4 (2014) 22509–22519.
- [53] E. R. Sacia, M. Balakrishnan, A. T. Bel, *J. Catal.*, 313 (2014) 70–79.
- [54] P. Lanzafame, G. Papanikolaou, S. Perathoner, G. Centi, M. Migliori, E. Catizzone, A. Aloise, G. Giordano, *Catal. Sci. Technol.*, 8 (2018) 1304–1313.
- [55] E.S. Vasiliadou, A.A. Lemonidou, *Chem. Eng. J.*, 231 (2013) 103–112.
- [56] V. Rekha, C. Sumana, S. Paul Douglas, N. Lingaiah, *Appl. Catal. A: Gen.*, 491 (2015) 155–162.
- [57] O. Levenspiel, *Chemical Reaction Engineering*, John Wiley & Sons, 1999. 47–48.